EDGE ARTICLE

Functional metal–organic framework boosting lithium metal anode performance *via* chemical interactions†

Wen Liu,[a] Yingying Mi,[ab] Zhe Weng,[a] Yiren Zhong,[a] Zishan Wu[a] and Hailiang Wang [iD] *[a]

Dendrite growth and low coulombic efficiency are two major factors that limit the utilization of Li metal electrodes in future generations of high-energy-density rechargeable batteries. This article reports the first study on metal–organic framework (MOF) materials for boosting the electrochemical performance of Li metal electrodes and demonstrates the power of molecular-structure functionalization for realizing desirable ion transport and Li metal nucleation and growth. We show that dendrite-free dense Li deposition and stable Li plating/stripping cycling with high coulombic efficiency are enabled by modifying a commercial polypropylene separator with a titanium-based MOF (NH_2-MIL-125(Ti)) material. The NH_2-MIL-125(Ti)-coated-separator renders Li|Cu cells that can run for over 200 cycles at 1 mA cm^{-2}–1 mA h cm^{-2} with average coulombic efficiency of 98.5% and Li|Li symmetric cells that can be cycled at 1 mA cm^{-2}–1 mA h cm^{-2} for more than 1200 h without short circuiting. The superior cycling stability is attributed to the amine substituents in the NH_2-MIL-125(Ti) structure which induce increased Li^+ transference numbers and uniform and dense early-stage Li deposition.

Introduction

Lithium ion batteries based on intercalation chemistry face substantial challenges in meeting the increasing energy density demand from modern electric vehicles and electrochemical energy storage.[1,2] As a potential solution, batteries with new chemistry beyond the Li ion intercalation technology, *e.g.* Li–S and $Li–O_2$ batteries, have attracted extensive attention because of their high energy densities.[3,4] Such rechargeable Li batteries use Li metal as the anode, which is essentially the ultimate form of high-capacity anode material for batteries based on Li ions. Despite their ultrahigh theoretical capacity (3860 mA h g^{-1}) and low standard electrode potential (−3.040 V *vs.* SHE), Li metal anodes suffer from low efficiency and short cycle life due to uncontrolled dendrite growth and side reactions with the electrolyte.[5–7] Sharp filaments of Li dendrites can pierce separators and cause an internal short circuit.[8–10] In addition, an unstable and thick solid electrolyte interlayer (SEI) is more likely to form

on Li moss or dendrites, which irreversibly consumes the Li ions in the electrolyte and hinders Li ion transportation during electrochemical processes.[11–13]

Many approaches have been explored to address these issues and unlock the full potential of Li metal anodes. Ceramic and polymer electrolytes with high mechanical strength have been used to suppress Li dendrite growth, though many solid electrolytes suffer from low ionic conductivities at ambient temperature as well as poor contact (high interfacial resistance) with electrodes.[14–22] For liquid electrolytes, their compositions are modified for facilitating uniform and stable SEI formation.[23–31] 3D structured Li anodes have been developed for achieving improved Li plating/stripping by reducing surface areal current densities.[32–35] Artificial interface layers have also been utilized to protect Li metal anodes during the electrochemical discharging/charging cycle.[36–39] Modification of separators, *e.g.* coating commercial separator membranes with various ceramic nanoparticles such as Al_2O_3, TiO_2, or h-BN, is another strategy to improve the cycling stability of Li metal anodes.[40–44] While these inorganic components can increase the mechanical strength of separators, they may also hamper Li ion diffusion; furthermore, they lack chemical interactions with the ions in the electrolyte to regulate Li ion transportation and redox. Although all the approaches have demonstrated effectiveness in improving the efficiency and cycle life of Li metal anodes to some extent, the achieved electrochemical performances are still far from the standards required for practical battery applications. New approaches and materials must be

[a]Department of Chemistry and Energy Sciences Institute, Yale University, 810 West Campus Drive, West Haven, CT 06516, USA. E-mail: hailiang.wang@yale.edu

[b]College of Chemistry and Molecular Engineering, Peking University, Beijing 100871, China

considered for further advancing the science and technology in the field.[45,46]

Here we for the first time demonstrate the utilization of metal–organic framework (MOF) structures for suppressing Li dendrite growth and increasing the cycling stability of Li metal anodes. By coating an NH_2-MIL-125(Ti) MOF material on a commercial separator membrane (Celgard 3501), we prepare a composite separator that can enable dendrite-free dense Li deposition and long-term reversible Li plating/stripping without introducing additional electrochemical resistance. With the MOF-decorated separator, we achieve more than 200 cycles of Li deposition and removal on Cu foil with average coulombic efficiency (CE) as high as 98.5%, under a current density of 1 mA cm^{-2} and a charging/discharging capacity of 1 mA h cm^{-2}. We also realize 1200 h of cycling for a symmetrical Li|Li cell under 1 mA cm^{-2} and 1 mA h cm^{-2} conditions. We further discover that the amine functional groups in the MOF structure make critical contributions to the superior electrochemical performance by interacting with the ions in the electrolyte, rendering higher Li ion transference numbers and inducing uniform Li nucleation and growth.

Results and discussion

NH_2-MIL-125(Ti) is an amine-functionalized form of the Ti-based MIL-125 MOF structure. The structure of MIL-125(Ti) is illustrated in Fig. S1.† The NH_2-MIL-125(Ti) structure features $Ti_8O_8(OH)_4$ nodes and 2-aminobenzene-1,4-dicarboxylate linkers (Fig. 1a and b), with two types of cages corresponding to the octahedral (~12.55 Å) and tetrahedral (~6.13 Å) interstitial sites of the close cubic packing. The triangular windows of the cages are in the size range of 5–7 Å.[47,48] The NH_2-MIL-125(Ti) was synthesized by a solvothermal method (see the ESI for experimental details†). The product exhibits a nanodisk-like morphology with an average diameter of 1.5 μm (Fig. S2a and b†). The X-ray diffraction (XRD) pattern shows a similar structure to that of MIL-125(Ti) (Fig. S2c†). The NH_2-MIL-125(Ti) material was coated onto a commercial polypropylene (PP) separator membrane to prepare the

composite separator (Fig. 1c). The surface morphology and microstructures of the pristine and coated separators were imaged with scanning electron microscopy (SEM). The MOF-decorated separator is fully covered with disk-shaped microparticles (Fig. 1e), clearly distinguishing it from the pristine separator with its macroporous structure (Fig. 1d). As shown by the cross-sectional image of the MOF-coated separator (Fig. 1f), the MOF layer is about 20 μm thick with the MOF particles adhering closely to the surface of the PP film.

Coin-type Li|Cu cells with pristine and NH_2-MIL-125(Ti)-coated separators were assembled to investigate electrochemical Li plating/stripping. 1 M lithium bis(trifluoromethane)sulfonimide (LiTFSI) in 1,3-dioxolane (DOL)/1,2-dimethoxyethane (DME) (1 : 1 volumetric ratio) solution with 2 wt% $LiNO_3$ additive was used as the electrolyte. The CE, namely the charge of Li removal with respect to that of Li deposition on Cu, was used as the performance index to evaluate the reaction reversibility and its stability upon cycling. The cells were first discharged and charged at a current density of 0.5 mA cm^{-2} with a cut-off capacity of 0.5 mA h cm^{-2} for 200 cycles, and then cycled under 1 mA cm^{-2}–1 mA h cm^{-2} conditions (Fig. 2a). For the Li|Cu cell with the pristine separator, an initial CE of 92% with an overpotential (defined as the difference between the charging and discharging potential plateaus) of 0.08 V was observed (Fig. 2a and b). After 20 cycles, the CE increased to 99% and the cell entered a steady-cycling state under the 0.5 mA cm^{-2}–0.5 mA h cm^{-2} conditions. However, 43 cycles after the cell entered the 1 mA cm^{-2}–1 mA h cm^{-2} cycling stage, the CE started to fluctuate violently due to a local internal short circuit of the cell. Incorporation of the MOF component significantly extends the cycle life of the Li metal anode. The Li|Cu cell with the NH_2-MIL-125(Ti)-coated separator was able to be stably cycled for 200 cycles at 0.5 mA cm^{-2}–0.5 mA h cm^{-2} followed by another 200 cycles at 1 mA cm^{-2}–1 mA h cm^{-2} (Fig. 2a). The initial CE of the cell was 94% with an overpotential of 0.21 V (Fig. 2a and c). After 10 discharging/charging cycles, the CE increased to 99% and the overpotential decreased to 0.08 V, which is comparable with that of the cell with the pristine separator. After 200 consecutive cycles at 0.5 mA cm^{-2}, the current density was increased to 1 mA cm^{-2}, and the cell maintained very low roundtrip capacity loss (average CE of 98.5%) with stable discharging/charging voltage profiles for another 200 cycles (Fig. 2c). The performance is among the best reported for Li|Cu cells working under equivalent conditions with other protecting strategies like 3D porous Cu,[49] interconnected hollow carbon nanospheres,[37] polymer films,[50] polymer fibers[51,52] and a Cu nanowire membrane,[53] most of which maintain high CE for 100–150 cycles at 1 mA cm^{-2} (Table S1†). At higher current densities of 1.5 and 3 mA cm^{-2}, the cell with the NH_2-MIL-125(Ti)-coated separator can be cycled at high efficiency for ~150 and 60 cycles, respectively (Fig. S3†). A Li|Cu cell with the NH_2-MIL-125(Ti)-coated separator but without the $LiNO_3$ additive in the electrolyte was also assembled and measured under 1 mA cm^{-2}–1 mA h cm^{-2} conditions. The cell had poor cycling stability with coulombic efficiency lower than 80% (Fig. S4†), suggesting that the MOF material cannot replace $LiNO_3$, likely in facilitating a stable SEI layer,[54] even though the
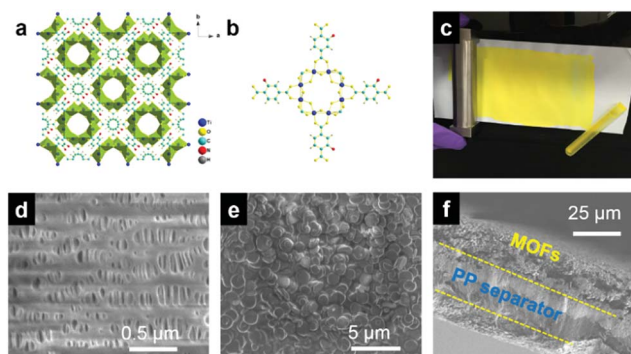

Fig. 1 MOF-decorated separator. (a) Illustration of the structure of NH_2-MIL-125(Ti). (b) One node of the MOF structure. (c) MOF film coated on PP separator membrane. (d) Top-view SEM image of the pristine separator. (e) Top-view SEM image of the MOF-decorated separator. (f) Cross-sectional view of MOF-decorated separator.
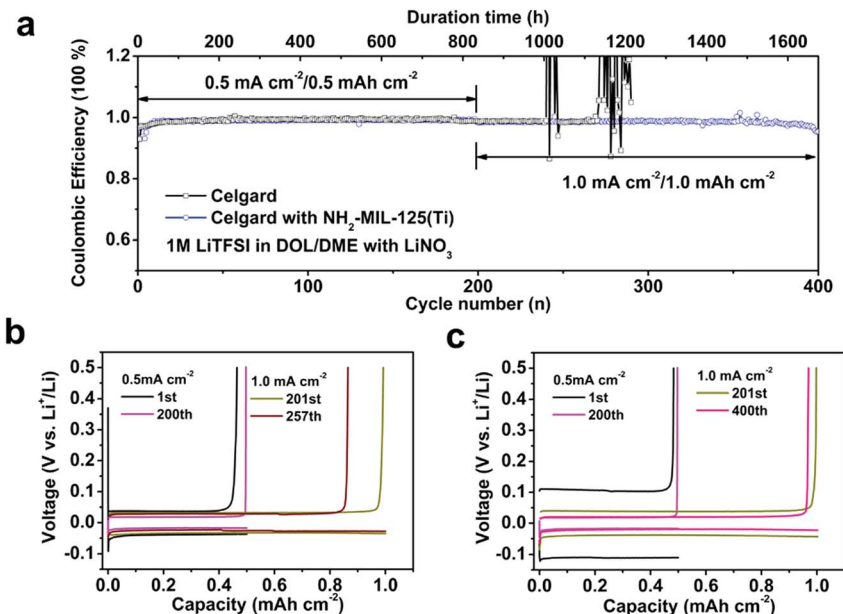
Fig. 2 Li|Cu cells with pristine and NH_2-MIL-125(Ti)-coated separators. (a) CE of consecutive Li plating/stripping cycles. The first 200 cycles were performed at a current density of 0.5 mA cm^{-2} with a cut-off capacity of 0.5 mA h cm^{-2}, and the following 200 cycles were under 1 mA cm^{-2}–1 mA h cm^{-2} conditions. (b) Voltage profiles for the cell with the pristine separator. (c) Voltage profiles for the cell with the NH_2-MIL-125(Ti)-coated separator.

MOF layer is highly effective in increasing efficiency and extending the cycle life in the presence of the LiNO$_3$ additive. The MOF-coated separator was also assessed with a carbonate electrolyte. While the cells generally exhibit lower CE than those with the ether based electrolyte, the cell with the NH$_2$-MIL-125(Ti)-coated separator still clearly outperforms that with the pristine separator (Fig. S5†).

We also fabricated symmetric Li|Li cells to further investigate the effect of NH$_2$-MIL-125(Ti) on the cycling stability of Li metal anodes. The cells were first cycled for 20 cycles at 0.25 mA cm^{-2}–0.5 mA h cm^{-2} followed by 20 cycles at 0.5 mA cm^{-2}–1.0 mA h cm^{-2} (Region I and II in Fig. 3a). Then the current density was increased to 1.0 mA cm^{-2} for long-term cycling with a cut-off capacity of 1 mA h cm^{-2} (Region III in Fig. 3a). The cell with
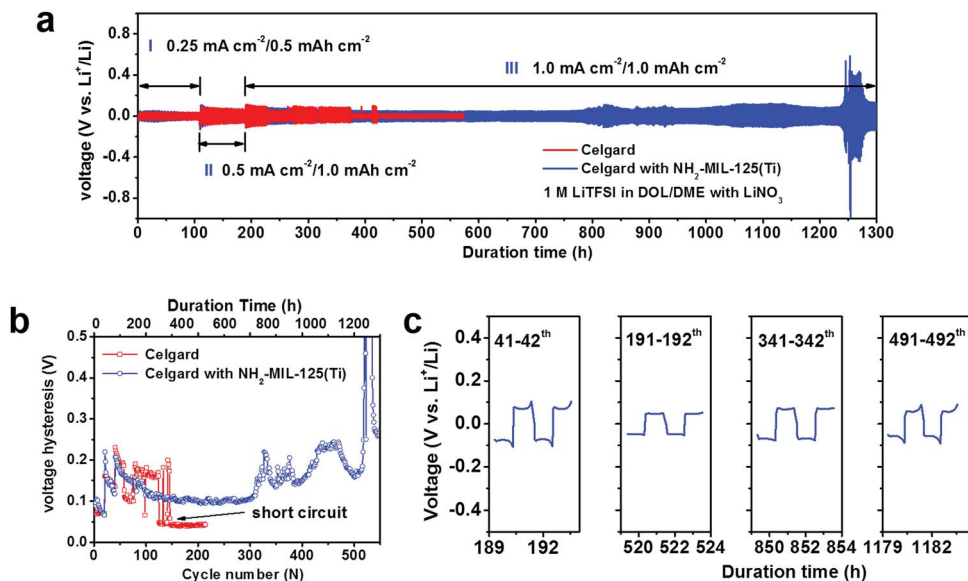

Fig. 3 Li|Li cells with pristine and NH_2-MIL-125(Ti)-coated separators. (a) Voltage profiles and (b) voltage hysteresis (difference between the voltage of Li stripping and that of Li plating) of Li metal plating/striping in symmetric Li|Li cells with pristine and NH_2-MIL-125(Ti)-coated separators. (c) Voltage profiles for specific cycles of the Li|Li cell with the NH_2-MIL-125(Ti)-coated separator. The electrolyte is 1 M LiTFSI in DOL/DME with 2% LiNO$_3$ additive.

the pristine separator could only be cycled under the 1 mA cm^{-2}–1 mA h cm^{-2} conditions for 86 cycles before it was short-circuited (Fig. 3a and b). In contrast, the cell with the NH_2-MIL-125(Ti)-coated separator could sustain stable cycling for more than 1200 h (Fig. 3a), corresponding to more than 500 consecutive cycles. Under equivalent cell configurations and measuring conditions, the cycling performance is favourably comparable to other Li|Li cells reported in the literature (Table S1†), placing our MOF-coated separators among the most effective approaches to stable Li metal electrodes operating with liquid electrolyte.

For the Li|Li cell with the NH_2-MIL-125(Ti) coated separator, the average voltage hysteresis of Li plating/stripping was 0.2 V at the start of the 1 mA cm^{-2}–1 mA h cm^{-2} cycling stage (Region III in Fig. 3a). It then gradually decreased to 0.1 V after about 100 cycles, and remained quite stable for 1200 h before a dramatic increase took place (Fig. 3b). The voltage profile was also quite stable throughout the long-term cycling measurement (Fig. 3c), indicating reversible Li plating/stripping. With another set of Li|Li cells, we monitored their electrochemical impedance over

cycling (Fig. S6†). The cell with the NH_2-MIL-125(Ti)-coated separator exhibited an initial charge transfer resistance of ~100 Ω, considerably higher than that of the cell with the pristine separator (~40 Ω). This is possibly due to insufficient and slow infiltration of the MOF pores with the liquid electrolyte at the initial stage. After 150 charging/discharging cycles, the resistance decreased to ~20 Ω and remained low throughout the rest of the 450 cycles.

We performed SEM imaging to examine the morphology and microstructure of Li deposited on Cu after 130 consecutive Li plating/stripping cycles (stopped after the Li plating step) at 0.5 mA cm^{-2} with a cut-off capacity of 1.0 mA h cm^{-2} (Fig. S7†). For the cell with the pristine separator, a Li layer of brown/black colour was observed on the Cu electrode (Fig. 4a). SEM imaging revealed extensive dendritic Li particles in the submicron size range (Fig. 4a and b). From the cross-sectional image, it is clear that the deposited Li layer has a loosely packed structure with a thickness >60 μm (Fig. 4c). In contrast, a shiny Li metal layer of silver/white colour was observed on the Cu electrode for the cell with the NH_2-MIL-125(Ti)-coated separator (Fig. 4d). The deposited Li layer comprises much larger particles (4 μm in diameter) with round edges (Fig. 4d and e). The cross-sectional image reveals that the deposited Li layer has a densely packed structure with a thickness of ~17 μm (Fig. 4f), which is only 1/4 of the thickness of the Li layer deposited under the pristine separator. Taken together, the NH_2-MIL-125(Ti) layer plays a key role in electrochemical Li deposition by rendering a compact Li layer of large particles with round edges. The reduced surface area is beneficial for suppressing parasitic side reactions on the exposed Li surface. The round and dense morphology also lowers the probability of piercing the separator. All these contribute to the observed superior cycling stability of the Li metal anode protected by the NH_2-MIL-125(Ti)-coated separator. The disassembled NH_2-MIL-125(Ti)-coated separator was analyzed by XRD. The result suggested that the MOF structure remained intact after 130 cycles (Fig. S8†).

To study the effect of MOF molecular structures on improving the cycling stability of Li metal anodes, we synthesized the MIL-125(Ti) MOF structure and compared the electrochemical performance of Li|Cu cells with pristine, MIL-125(Ti)-coated and NH_2-MIL-125(Ti)-coated separators at
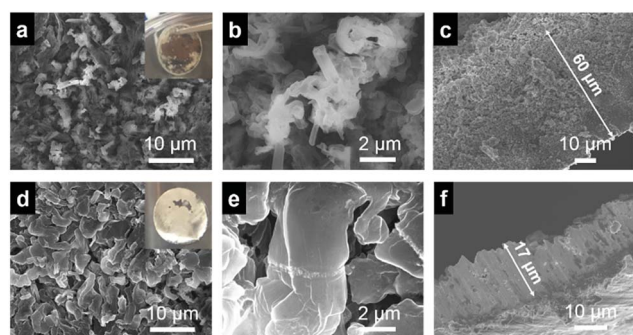

Fig. 4 Morphology of Li metal deposited on Cu electrode after 130 cycles under 0.5 mA cm^{-2}–1.0 mA h cm^{-2} conditions. (a, b) Top-view SEM images of Li deposited on Cu in the cell with the pristine separator. Inset of (a) is a digital photo of the Li layer on Cu. (c) Cross-sectional SEM image of the deposited Li layer under the pristine separator. (d, e) Top-view SEM images of Li deposited on Cu in the cell with the NH_2-MIL-125(Ti)-coated separator. Inset of (d) is a digital photo of the Li layer on Cu. (f) Cross-sectional SEM image of the deposited Li layer in the cell with the NH_2-MIL-125(Ti)-coated separator.
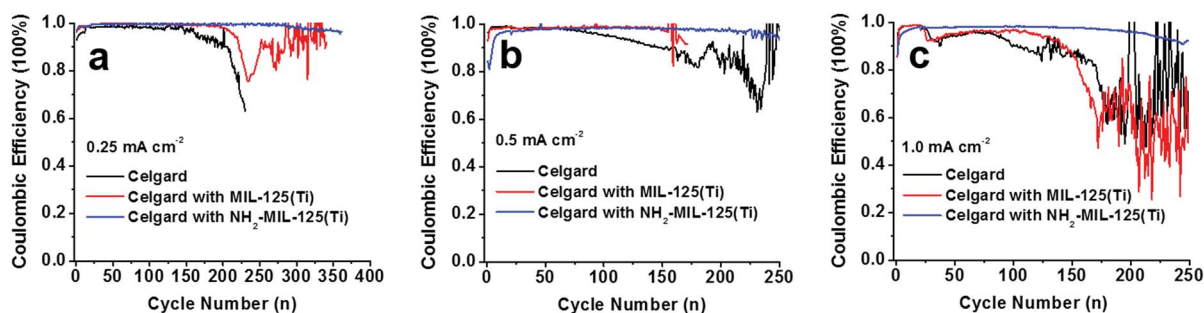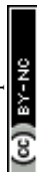

Fig. 5 Electrochemical performance of Li|Cu cells with pristine, MIL-125(Ti)-coated and NH_2-MIL-125(Ti)-coated separators at various current densities. CE of Li plating/stripping at (a) 0.25, (b) 0.5 and (c) 1.0 mA cm^{-2}, with a cut-off capacity of 1.0 mA h cm^{-2}. Electrolyte used is 1 M LiTFSI in DOL/DME with 2% $LiNO_3$ additive.

various current densities with a cut-off capacity of 1.0 mA h cm^{-2} (Fig. 5 and S9†). At a low current density of 0.25 mA cm^{-2}, the cell with the pristine separator lasted for about 150 cycles before the CE started to drop significantly (Fig. 5a). The cell with the MIL-125(Ti)-coated separator maintained a high CE for more than 200 cycles, outperforming the one with the pristine separator, but being considerably inferior to the cell with the NH$_2$-MIL-125(Ti)-coated separator which showed more than 300 stable cycles with an average CE of 99.0% (Fig. 5a). The same trend in cycling stability was found at higher current densities. At 0.5 mA cm^{-2}, the two cells with the pristine and the MIL-125(Ti)-coated separators lasted for 100 and 150 cycles with CE >95.0%, respectively, while the cell with the NH$_2$-MIL-125(Ti)-coated separator was able to run for 250 cycles with an average CE of 98.2% (Fig. 5b). At 1 mA cm^{-2}, the cell with the NH$_2$-MIL-125(Ti)-coated separator was stably cycled for 220 cycles with an average CE of 97.5%, outperforming the other two cells with the pristine and MIL-125(Ti)-coated separators which lasted for only 85 and 118 cycles before the CE dropped below 95.0% (Fig. 5c). The results clearly demonstrate that the amine functional groups in the NH$_2$-MIL-125(Ti) MOF structure play a key role in boosting the Li metal anode performance.

To understand how the NH$_2$-MIL-125(Ti) MOF regulates electrochemical Li deposition and enhances Li plating/stripping cycling stability, we measured the Li ion transference numbers (t_{Li^+}) associated with the three different separators filled with liquid electrolyte. The transference numbers were measured from Li|Li symmetric cells with AC impedance (Fig. S10†) and potential impulse techniques (Fig. 6a–c, see the ESI for experimental details†).[55] With the pristine separator, the Li ion transference number was 0.49–0.59 (Fig. 6a), agreeing well with the values reported in the literature for the same electrolyte.[55] Switching to the MIL-125(Ti)-coated separator did not change the Li ion transference number (Fig. 6b), indicating that the MIL-125(Ti) MOF structure has negligible interactions with the ions in the electrolyte. With the NH$_2$-MIL-125(Ti)-coated separator, the Li ion transference number increased significantly to 0.64–0.78 (Fig. 6c). We believe the increased Li ion transference number is due to interactions between the amine groups of the NH$_2$-MIL-125(Ti) MOF structure and the ions in the electrolyte. In the literature there have been reports on modified separators that induce increased Li$^+$ transference numbers.[56–58] Amine groups are regarded as strongly interactive with ions, thereby facilitating dissociation of ion pairs and promoting Li$^+$ transport.[58,59] However, the exact interaction mechanism has still yet to be revealed.

During electrochemical Li deposition, the negatively polarized Li metal surface provides electrons to reduce the adjacent Li cations for Li metal plating. As the lithium cations are consumed by reduction and the anions are expelled by the electric field, an ion depletion layer forms. When the ionic concentration near the electrode surface drops to zero after a certain time (Sand's time), the electroneutrality is violated and the local space charge leads to nucleation and growth of Li dendrites.[60,61] Li ion flux to sustain
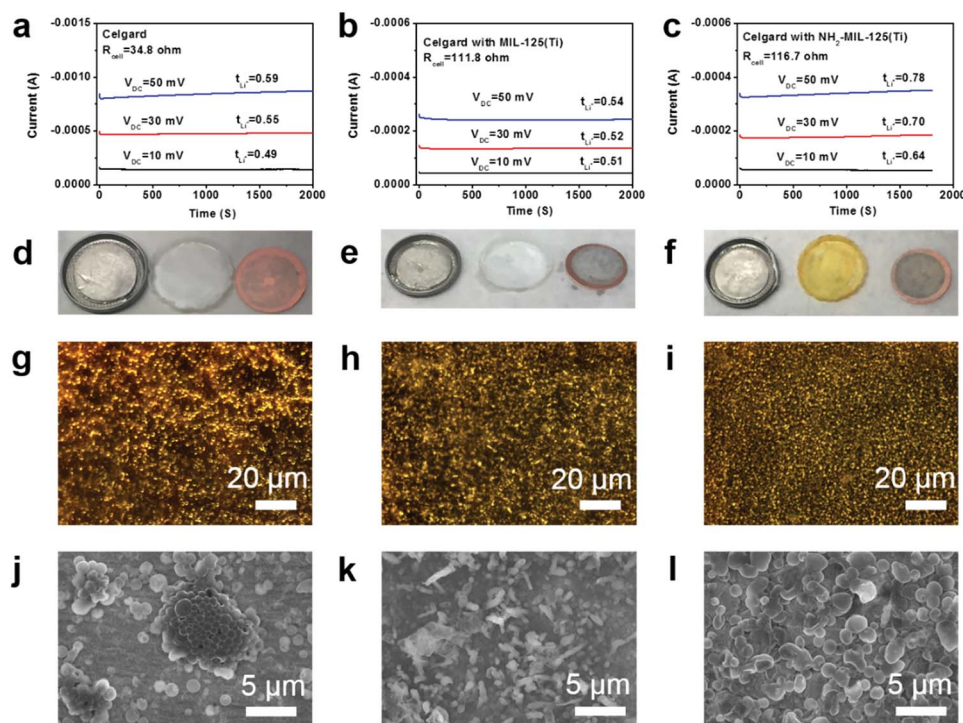

Fig. 6 Li ion transference number and early-stage Li metal deposition. Steady-state current measurements and Li ion transference numbers for (a) pristine separator, (b) MIL-125(Ti)-coated and (c) NH$_2$-MIL-125(Ti)-coated separator filled with 1.0 M LiTFSI in DOL/DME with 2% LiNO$_3$. (d–f) Digital photos, and (g–i) optical microscopy and (j–l) SEM images of deposited Li metal for disassembled Li|Cu cells with (d, g and j) pristine separator, (e, h and k) MIL-125(Ti)-coated and (f, i and l) NH$_2$-MIL-125(Ti)-coated separator. Li deposition was performed for the cells at 0.5 mA cm^{-2} for 15 min.

mass transport and subsequent reduction is therefore important for dendrite-free Li metal deposition. Compared with the pristine and MIL-125(Ti)-coated separators, the NH_2-MIL-125(Ti)-coated separator renders higher t_{Li^+} and thus lower t_{anion}, leading to a longer Sand's time.[7,60,62] As a result, with the same electrolyte, Li ion transportation in the cell with the NH_2-MIL-125(Ti)-coated separator is more effective in maintaining uniform Li metal deposition.

To further verify this hypothesis, we conducted short-time Li deposition (0.5 mA cm^{-2} for 15 min) for the Li|Cu cells with different separators and then imaged the Cu electrodes with optical microscopy and SEM. The Cu electrode of the cell with the pristine separator was nonuniformly covered with Li crystallites (Fig. 6d and g). Sparse Li protrusions can be seen in the SEM image (Fig. 6j). Such non-uniform early-stage Li deposition is likely to result in dendritic growth since subsequent deposition will preferably occur at the protrusions. In fact, sparse nucleation has been proved to be a successful strategy for growing anisotropic structures such as nanowires or dendrites in metal electrodeposition.[63] For lithium deposition with the MIL-125(Ti)-coated separator, more evenly distributed Li deposition was observed (Fig. 6e and h). However, the Li layer showed a mossy rod-like morphology (Fig. 6k). In contrast, the deposited Li in the NH_2-MIL-125(Ti)-containing cell appeared to be a uniform layer (Fig. 6f and i) with densely packed round particles (Fig. 6l). Such a morphology in the early stage of Li deposition can support uniform and compact Li growth, and thus alleviate side reactions with the electrolyte and reduce the probability of short circuit.

Conclusions

We have for the first time investigated using MOF materials and their molecular structure functionalization to facilitate stabilized cycling of Li metal anodes. Coating separators with NH_2-MIL-125(Ti) enables long-cycle-life Li|Cu and Li|Li cells with dendrite-free Li deposition and high-efficiency Li plating/stripping. The high electrochemical performance is attributed to higher Li$^+$ transference numbers and uniform Li nucleation as a result of the interactions between the electrolyte and the NH_2 groups in the MOF structure. This study provides a new approach of utilizing MOF materials for Li anode protection and highlights the influence of substituents in the molecular structures on electrode performance.

Acknowledgements

Notes and references

1 M. Armand and J. M. Tarascon, *Nature*, 2008, **451**, 652–657.

2 J. W. Choi and D. Aurbach, *Nat. Rev. Mater.*, 2016, **1**, 16013.

3 P. G. Bruce, S. A. Freunberger, L. J. Hardwick and J.-M. Tarascon, *Nat. Mater.*, 2012, **11**, 19–29.

4 R. Cao, W. Xu, D. Lv, J. Xiao and J. G. Zhang, *Adv. Energy Mater.*, 2015, **5**, 1402273.

5 X. B. Cheng, R. Zhang, C. Z. Zhao, F. Wei, J. G. Zhang and Q. Zhang, *Adv. Sci.*, 2016, **3**, 1500213.

6 K. Zhang, G. H. Lee, M. Park, W. Li and Y. M. Kang, *Adv. Energy Mater.*, 2016, 1600811, DOI: 10.1002/aenm.201600811.

7 M. D. Tikekar, S. Choudhury, Z. Tu and L. A. Archer, *Nat. Energy*, 2016, **1**, 16114.

8 J. Yamaki, S. Tobishima, K. Hayashi, S. Keiichi, Y. Nemoto and M. Arakawa, *J. Power Sources*, 1998, **74**, 219–227.

9 L. Gireaud, S. Grugeon, S. Laruelle, B. Yrieix and J. M. Tarascon, *Electrochem. Commun.*, 2006, **8**, 1639–1649.

10 J. Steiger, D. Kramer and R. Mönig, *J. Power Sources*, 2014, **261**, 112–119.

11 D. Aurbach, A. Zaban, Y. Gofer, Y. E. Ely, I. Weissman, O. Chusid and O. Abramson, *J. Power Sources*, 1995, **54**, 76–84.

12 A. Tudela Ribes, P. Beaunier, P. Willmann and D. Lemordant, *J. Power Sources*, 1996, **58**, 189–195.

13 K. Morigaki, *J. Power Sources*, 2002, **104**, 13–23.

14 P. Lightfoot, M. A. Mehta and P. G. Bruce, *Science*, 1993, **262**, 883–885.

15 X. Yu, *J. Electrochem. Soc.*, 1997, **144**, 524.

16 F. Croce, G. B. Appetecchi, L. Persi and B. Scrosati, *Nature*, 1998, **394**, 456–458.

17 D. R. MacFarlane, J. Huang and M. Forsyth, *Nature*, 1999, **402**, 792–794.

18 M. Rosso, T. Gobron, C. Brissot, J. N. Chazalviel and S. Lascaud, *J. Power Sources*, 2001, **97–98**, 804–806.

19 N. Kamaya, K. Homma, Y. Yamakawa, M. Hirayama, R. Kanno, M. Yonemura, T. Kamiyama, Y. Kato, S. Hama, K. Kawamoto and A. Mitsui, *Nat. Mater.*, 2011, **10**, 682–686.

20 R. Bouchet, S. Maria, R. Meziane, A. Aboulaich, L. Lienafa, J. P. Bonnet, T. N. Phan, D. Bertin, D. Gigmes, D. Devaux, R. Denoyel and M. Armand, *Nat. Mater.*, 2013, **12**, 452–457.

21 Y. Wang, W. D. Richards, S. P. Ong, L. J. Miara, J. C. Kim, Y. Mo and G. Ceder, *Nat. Mater.*, 2015, **14**, 1026–1031.

22 Y. Lu, M. Tikekar, R. Mohanty, K. Hendrickson, L. Ma and L. A. Archer, *Adv. Energy Mater.*, 2015, **5**, 1402073.

23 K. Saito, Y. Nemoto, S. Tobishima and J. Yamaki, *J. Power Sources*, 1997, **68**, 476–479.

24 O. Crowther and A. C. West, *J. Electrochem. Soc.*, 2008, **155**, A806.

25 Y. Zhang, J. Qian, W. Xu, S. M. Russell, X. Chen, E. Nasybulin, P. Bhattacharya, M. H. Engelhard, D. Mei, R. Cao, F. Ding, A. V. Cresce, K. Xu and J. G. Zhang, *Nano Lett.*, 2014, **14**, 6889–6896.

26 Y. Lu, Z. Tu and L. A. Archer, *Nat. Mater.*, 2014, **13**, 961–969.

27 J. Qian, W. A. Henderson, W. Xu, P. Bhattacharya, M. Engelhard, O. Borodin and J. G. Zhang, *Nat. Commun.*, 2015, **6**, 6362.

28 W. Li, H. Yao, K. Yan, G. Zheng, Z. Liang, Y. M. Chiang and Y. Cui, *Nat. Commun.*, 2015, **6**, 7436.

29 A. Basile, A. I. Bhatt and A. P. O'Mullane, *Nat. Commun.*, 2016, **7**, 11794.

30 C. Zu, A. Dolocan, P. Xiao, S. Stauffer, G. Henkelman and A. Manthiram, *Adv. Energy Mater.*, 2016, **6**, 1501933.

31 X. Q. Zhang, X. B. Cheng, X. Chen, C. Yan and Q. Zhang, *Adv. Funct. Mater.*, 2017, **27**, 1605989.

32 X. B. Cheng, H. J. Peng, J. Q. Huang, R. Zhang, C. Z. Zhao and Q. Zhang, *ACS Nano*, 2015, **9**, 6373–6382.

33 Z. Liang, D. Lin, J. Zhao, Z. Lu, Y. Liu, C. Liu, Y. Lu, H. Wang, K. Yan, X. Tao and Y. Cui, *Proc. Natl. Acad. Sci. U. S. A.*, 2016, **113**, 2862–2867.

34 R. Zhang, X. B. Cheng, C. Z. Zhao, H. J. Peng, J. L. Shi, J. Q. Huang, J. Wang, F. Wei and Q. Zhang, *Adv. Mater.*, 2016, **28**, 2155–2162.

35 Y. Sun, G. Zheng, Z. W. Seh, N. Liu, S. Wang, J. Sun, H. R. Lee and Y. Cui, *Chem*, 2016, **1**, 287–297.

36 S. M. Choi, I. S. Kang, Y. K. Sun, J. H. Song, S. M. Chung and D. W. Kim, *J. Power Sources*, 2013, **244**, 363–368.

37 G. Zheng, S. W. Lee, Z. Liang, H. W. Lee, K. Yan, H. Yao, H. Wang, W. Li, S. Chu and Y. Cui, *Nat. Nanotechnol.*, 2014, **9**, 618–623.

38 H. Lee, D. J. Lee, Y. J. Kim, J. K. Park and H. T. Kim, *J. Power Sources*, 2015, **284**, 103–108.

39 N. W. Li, Y. X. Yin, C. P. Yang and Y. G. Guo, *Adv. Mater.*, 2016, **28**, 1853–1858.

40 H. Volker, H. Christian and H. Gerhard, US7807286 B2, 2010.

41 Z. Zhang, Y. Lai, Z. Zhang, K. Zhang and J. Li, *Electrochim. Acta*, 2014, **129**, 55–61.

42 Z. Y. Tu, Y. Kambe, Y. Y. Lu and L. A. Archer, *Adv. Energy Mater.*, 2014, **4**, 1300654.

43 W. Luo, L. Zhou, K. Fu, Z. Yang, J. Wan, M. Manno, Y. Yao, H. Zhu, B. Yang and L. Hu, *Nano Lett.*, 2015, **15**, 6149–6154.

44 Z. Tu, M. J. Zachman, S. Choudhury, S. Wei, L. Ma, Y. Yang, L. F. Kourkoutis and L. A. Archer, *Adv. Energy Mater.*, 2017, 1602367, DOI: 10.1002/aenm.201602367.

45 B. M. Wiers, M. L. Foo, N. P. Balsara and J. R. Long, *J. Am. Chem. Soc.*, 2011, **133**, 14522–14525.

46 S. Bai, X. Liu, K. Zhu, S. Wu and H. Zhou, *Nat. Energy*, 2016, **1**, 16094.

47 M. Dan Hardi, C. Serre, T. Frot, L. Rozes, G. Maurin, C. Sanchez and G. Férey, *J. Am. Chem. Soc.*, 2009, **131**, 10857–10859.

48 C. Zlotea, D. Phanon, M. Mazaj, D. Heurtaux, V. Guillerm, C. Serre, P. Horcajada, T. Devic, E. Magnier, F. Cuevas, G. Ferey, P. L. Llewellyn and M. Latroche, *Dalton Trans.*, 2011, **40**, 4879–4881.

49 Q. Yun, Y. B. He, W. Lv, Y. Zhao, B. Li, F. Kang and Q. H. Yang, *Adv. Mater.*, 2016, **28**, 6932–6939.

50 B. Zhu, Y. Jin, X. Hu, Q. Zheng, S. Zhang, Q. Wang and J. Zhu, *Adv. Mater.*, 2016, DOI: 10.1002/adma.201603755.

51 Z. Liang, G. Zheng, C. Liu, N. Liu, W. Li, K. Yan, H. Yao, P. C. Hsu, S. Chu and Y. Cui, *Nano Lett.*, 2015, **15**, 2910–2916.

52 X. B. Cheng, T. Z. Hou, R. Zhang, H. J. Peng, C. Z. Zhao, J. Q. Huang and Q. Zhang, *Adv. Mater.*, 2016, **28**, 2888–2895.

53 L. L. Lu, J. Ge, J. N. Yang, S. M. Chen, H. B. Yao, F. Zhou and S. H. Yu, *Nano Lett.*, 2016, **16**, 4431–4437.

54 D. Aurbach, E. Pollak, R. Elazari, G. Salitra, C. S. Kelley and J. Affinito, *J. Electrochem. Soc.*, 2009, **156**, A694–A702.

55 L. Suo, Y. S. Hu, H. Li, M. Armand and L. Chen, *Nat. Commun.*, 2013, **4**, 1481.

56 W. Xu, Z. Wang, L. Shi, Y. Ma, S. Yuan, L. Sun, Y. Zhao, M. Zhang and J. Zhu, *ACS Appl. Mater. Interfaces*, 2015, **7**, 20678–20686.

57 J. Song, H. Lee, M. J. Choo, J. K. Park and H. T. Kim, *Sci. Rep.*, 2015, **5**, 14458.

58 R. Zahn, M. F. Lagadec, M. Hess and V. Wood, *ACS Appl. Mater. Interfaces*, 2016, **8**, 32637–32642.

59 R. P. Doyle, X. Chen, M. Macrae, A. Srungavarapu, L. J. Smith, M. Gopinadhan, C. O. Osuji and S. Granados-Focil, *Macromolecules*, 2014, **47**, 3401–3408.

60 H. J. S. Sand, *Philos. Mag.*, 1901, **1**, 45–79.

61 P. Bai, J. Li, F. R. Brushett and M. Z. Bazant, *Energy Environ. Sci.*, 2016, **9**, 3221–3229.

62 W. Xu, J. Wang, F. Ding, X. Chen, E. Nasybulin, Y. Zhang and J. G. Zhang, *Energy Environ. Sci.*, 2014, **7**, 513–537.

63 L. P. Bicelli, B. Bozzini, C. Mele and L. D'Urzo, *Int. J. Electrochem. Sci.*, 2008, **3**, 356–408.